Comprehensive spectral analysis of Cyg X-1 using *RXTE* data

Rizwan Shahid[1], Ranjeev Misra[2] and S. N. A. Jaaffrey[1]

[1] Department of Physics, M. L. Sukhadia University, Udaipur-313001, India;

[2] Inter University Centre for Astronomy and Astrophysics, Pune-411007, India;
rmisra@iucaa.ernet.in

Abstract We analyze a large number (> 500) of pointed *Rossi X-Ray Timing Explorer (RXTE)* observations of Cyg X-1 and model the spectrum of each one. A subset of the observations for which there is a simultaneous reliable measure of the hardness ratio by the All Sky Monitor shows that the sample covers nearly all the spectral shapes of Cyg X-1. Each observation is fitted with a generic empirical model consisting of a disk black body spectrum, a Comptonized component whose input photon shape is the same as the disk emission, a Gaussian to represent the iron line and a reflection feature. The relative strength, width of the iron line and the reflection parameter are in general correlated with the high energy photon spectral index Γ. This is broadly consistent with a geometry where for the hard state (low $\Gamma \sim 1.7$) there is a hot inner Comptonizing region surrounded by a truncated cold disk. The inner edge of the disk moves inwards as the source becomes softer till finally in the soft state (high $\Gamma > 2.2$) the disk fills the inner region and active regions above the disk produce the Comptonized component. However, the reflection parameter shows non-monotonic behavior near the transition region ($\Gamma \sim 2$), which suggests a more complex geometry or physical state of the reflector. In addition, the inner disk temperature, during the hard state, is on average higher than in the soft one, albeit with large scatter. These inconsistencies could be due to limitations in the data and the empirical model used to fit them. The flux of each spectral component is well correlated with Γ, which shows that unlike some other black hole systems, Cyg X-1 does not show any hysteresis behavior. In the soft state, the flux of the Comptonized component is always similar to the disk one, which confirms that the ultra-soft state (seen in other brighter black hole systems) is not exhibited by Cyg X-1. The rapid variation of the Compton amplification factor with Γ naturally explains the absence of spectra with $\Gamma < 1.6$, despite a large number having $\Gamma \sim 1.65$. This comprehensive analysis lays the framework by which more detailed and sophisticated broadband observations may be understood.

Key words: accretion, accretion disks — X-rays: binaries

1 INTRODUCTION

Over the last forty years, several generations of X-ray satellites have observed Cyg X-1, which make it one of the best studied black hole systems. The source is known to undergo spectral state transitions between a hard/low state and a soft/high state. Historically, most of the time, the source

is found in the hard state which can be approximately characterized as a hard power-law emission with a high energy cutoff at ~ 100 keV. The basic model invoked to explain the hard state is that of a truncated cold standard accretion disk with a hot inner region (Shapiro et al. 1976). In this geometry, photons from the outer truncated disk impinge into the hot inner region and produce the observed Comptonization spectrum. This generic model has been refined by the formulation of theoretically more consistent and stable hot inner disks (e.g. Narayan & Yi 1994; Esin et al. 1998) and by a more detailed spectral modeling which includes the effect of reflection and possible non-thermal emission (see Gierlinski et al. 1997). An alternate interpretation of the hard state is that there is an extended transition region where the temperature increases rapidly and the emergent spectrum is the sum of the local spectra of each radius (Misra et al. 1997; Misra 2000).

In contrast, the soft state is dominated by a thermal emission and a steep hard X-ray emission extending to at least several hundred keV. In analogy with the solar corona, the basic model for the soft state is that of a cold accretion disk extending to the last stable orbit with a hot corona on top (Liang & Price 1977). More consistent modeling comprised of active regions or blobs on top of the cold disk have been formulated (for example Haardt et al. 1994) and detailed spectral modeling of this state, including reflection and non-thermal emission, have been undertaken (Gierliński et al. 1999). Done et al. (2007) present a review of the present understanding of the accretion process in such systems.

Cyg X-1 shows these two spectral states and transitions between them which are sometimes referred to an intermediate state (e.g. Malzac et al. 2006). Other black holes systems, in particular GRS 1915+105, show a myriad of spectral states whose classification also depends on the temporal property of the source (e.g. Belloni et al. 1997; Dunn et al. 2010; Zdziarski & Gierliński 2004; Remillard & McClintock 2006). These other black hole systems also exhibit a very high or ultra-soft state, where the spectrum is dominated by the thermal emission and the power-law emission is weak. This ultra-soft state has never been observed for Cyg X-1. Overall, the spectral behavior of Cyg X-1 is simpler than that in other black hole systems and hence its systematic analysis may pave the way for a better understanding of black hole systems in general.

For more than a decade, the *Rossi X-ray Timing Experiment (RXTE)*, with its Proportional Counter Array (PCA) and High Energy X-ray Timing Experiment (HEXTE), has provided unprecedented coverage of Cyg X-1. The high time resolution and large effective area of the PCA has provided a wealth of information regarding the rapid variability of black hole systems. For Cyg X-1, the shape of the power spectra and the discovery of frequency dependent time lags between different energy bands (Nowak et al. 1999) have indicated that the variability is due to propagation of waves in the disk (Lyubarskii 1997; Nowak et al. 1999; Titarchuk et al. 2007; Misra & Zdziarski 2008; Misra 2000; Kotov et al. 2001). Detailed power spectral analyses of Cyg X-1 using a number of *R*XTE observations have been undertaken (Pottschmidt et al. 2003; Axelsson et al. 2005).

Detailed photon spectral studies of specific observations of Cyg X-1 by *R*XTE have been undertaken in the hard and soft states, as well as in the transition phase (e.g. Gierlinski et al. 1997; Gierliński et al. 1999; Malzac et al. 2006; Nowak et al. 2011). The large number of observations of the source by *R*XTE allows for a more comprehensive study of its spectral properties and correlations between them. Ibragimov et al. (2005) undertook a detailed spectral study of 42 *Ginga-R*XTE and *RXTE*-OSSE observations, but these observations were limited to the hard state. Recently, in a brief report, Gierlinski et al. (2010) performed a detailed analysis of the spectral and timing properties of 33 representative *RXTE* observations covering the different spectral shapes of Cyg X-1.

Wilms et al. (2006) have analyzed the spectra of ~ 200 pointed *RXTE* observations of Cyg X-1, and have fitted them with an empirical broken power-law and thermal Comptonization models, with reflection and iron line emission. They caution that since the empirical broken power-law model is a reasonable fit to the data, more complicated models could be a case of "overparameterizing." In particular, they state that the broad iron line feature could be an artifact caused by fitting an incorrect simple thermal model to the soft excess component. This indeed is true given the energy resolution

of the *RXTE* instruments and the systematic uncertainties in their response. However, as discussed above, in the standard paradigm, the standard accretion disks in black hole systems extend to the last stable orbit in the soft state and a broad iron line is expected from such a system. Moreover, although Wilms et al. (2006) analyzed ~ 200 observations, these may not cover the entire range of spectral shapes exhibited by Cyg X-1.

In this work, we analyze 504 pointed *RXTE* observations of Cyg X-1 and fit the spectra of each one with a uniform model. We show that this large number of observations represents nearly all the spectral shapes of Cyg X-1. Our motivation is to verify the standard paradigms of the geometry of the hard and soft states, by studying the correlation between different spectral components and to bring out any discrepancies or complexities in the spectral evolution.

2 THE *RXTE* SAMPLE

Over the last 14 years, the *All-Sky Monitor* (ASM) of *RXTE* has provided extensive coverage of Cyg X-1. We obtained the ASM light-curves from *http://xte.mit.edu/ASM_lc.html*, using the standard filtering criteria mentioned there. One-day average light-curves were obtained and the hardness ratio, H, between the C (5–12.2 keV) and B (3–5 keV) energy bands were computed. For 4781 daily averages, the hardness ratios have a 1-sigma error less than 10% and the histogram of these data is shown in Figure 1 (solid line). There are two clear peaks in the distribution corresponding to the hard ($H \sim 1.5$) and soft ($H \sim 0.6$) states.
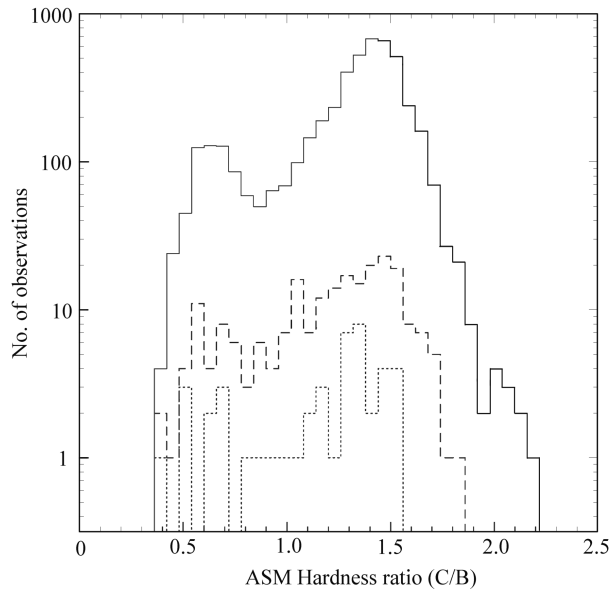

Fig. 1 The distributions of the ASM hardness ratio $H = C/B$ between the C (5–12.2 keV) and B (3–5 keV) energy bands. The solid line represents all the one-day average detections for which H has a 1-sigma error less than 10%. The dashed line represents 221 of the 504 pointed observations, analyzed in this work, for which there are simultaneous ASM dwell data and for which the average hardness in the ASM band has errors less than 10%. These observations scan nearly the entire range of hardness detected by the ASM. The dotted line represents 49 of the 200 pointed observations of the Wilms et al. (2006) analysis for which there are simultaneous ASM dwell data.

In this work, we have analyzed the spectra of 504 pointed observations of *RXTE*, and 221 of these observations have simultaneous ASM dwell data, whose average hardness ratio could be estimated with an uncertainty less than 10%. The distribution of their hardness ratio is plotted in Figure 1 (dashed line). The figure shows that the range $0.35 < H < 1.85$ covered by these pointed observations is nearly the entire range observed by ASM, except for some rare observations with $H > 1.8$. There are no simultaneous pointed observations during the time when the ASM detected $H > 1.8$. Thus the sample of pointed observations analyzed in this work covers nearly the entire range of spectral variability of Cyg X-1. As a comparison, the dotted line in Figure 1 represents the 49 observations of the sample analyzed by Wilms et al. (2006) which has simultaneous ASM data.

The pointed observations which have simultaneous ASM detections can be used to calibrate the ASM count rate and to understand any time-dependent systematics that the instrument may have. This in turn will allow for the study of the long term (days to months) variability of the source in conjunction with the spectral properties. We defer that exercise to a latter work, and here we concentrate instead on the PCA/HEXTE spectral analysis.

3 SPECTRAL ANALYSIS

For 504 *RXTE* pointed observations of Cyg X-1, we use the spectral and response files for the PCA and HEXTE data, that have been generated for the standard products using a general script[1]. Although the general script may not be optimized for a single observation, it is appropriate for this work, where the sample properties of a large number of observations are being studied. We fit the PCA data in the energy range $3 - 20$ keV, while for HEXTE the chosen range was $20 - 80$ keV. A systematic uncertainty of 0.01 was included in all fits (Jahoda et al. 2006).

All the observations were fitted by a generic model consisting of a multi-color disk black body and a hot thermal plasma which Comptonizes the disk photons. The model includes reflection and an iron line. In terms of XSPEC routines, the model is described as *wabs* (*diskbb* + *reflect*(*nthcomp*) + *Gaussian*). Since the PCA energy band is > 3 keV, the column density of the absorption component (wabs) cannot be constrained and hence was fixed at a negligible value of 10^{21} cm^{-2}. The disk's black body emission (*diskbb*) is parameterized by the inner disk temperature, $kT_{\rm in}$. In the thermal Comptonization model, *nthcomp* (Zdziarski et al. 1996; Życki et al. 1999), the input photon spectrum is taken to be the disk's black body shape and its temperature is tied to $kT_{\rm in}$. The thermal Comptonized spectrum is parameterized by the electron temperature $kT_{\rm e}$ and the high energy spectral index, Γ. Since HEXTE is not sensitive enough to detect the high energy turnover in the spectrum, the temperature was fixed at $kT_{\rm e} = 100$ keV. We have checked that our results are insensitive as long as $kT_{\rm e} > 50$ keV. The iron line was represented by a variable width Gaussian with centroid energy fixed at 6.4 keV. Finally, a convolution model (*reflect*) produces the reflected component of the incident X-ray photons from the accretion disk. Apart from the three normalization factors for the additive models, the parameters of this generic model are the inner disk temperature $kT_{\rm in}$, the high energy photon spectral index Γ, the reflection fraction R and the width of the Gaussian line, σ. The model was fit to all the observations and errors ($\Delta\chi^2 = 2.7$) for these parameters were computed. The presence of the convolution model for reflection and the large number of observations made the spectral fitting process computer intensive and extremely time consuming.

Although physically motivated, the generic model is basic and does not incorporate several important effects. For example, the intrinsic absorption in the source could be as high as a few $\times10^{21}$ cm^{-2} (e.g. Feng & Cui 2002), but we do not consider the effect here. Moreover, there could be a component of non-thermal electrons in the hot plasma, especially in the soft state of the source. The reflected component is assumed to be from neutral material, but in general it may be ionized. The iron line modeled as a Gaussian is an approximation to more realistic models which take into account the skewed nature of the line profile due to gravitational effects. However, as shown below,

---

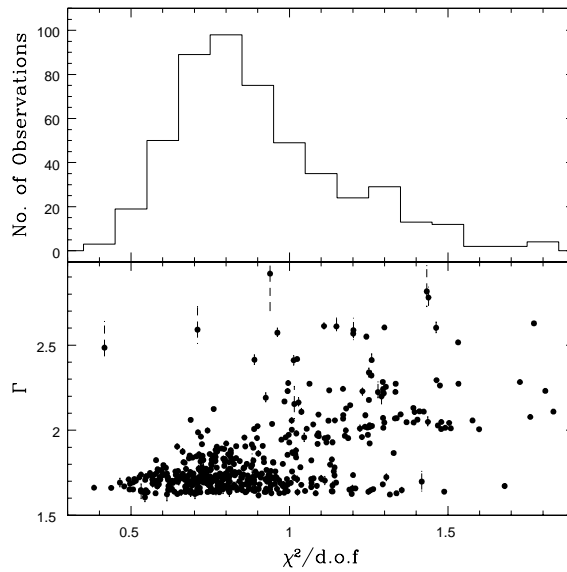[1] *http://heasarc.gsfc.nasa.gov/docs/xte/recipes/stdprod_guide.html*

Fig. 2 *Top Panel*: The distribution of observations as a function of reduced $\chi^2_{\rm red} = \chi^2/{\rm d.o.f.}$ The peak of the distribution is at ~ 0.8 and for all observations $\chi^2_{\rm red} < 1.9$. *Bottom Panel*: The variation of the photon spectral index Γ with $\chi^2_{\rm red}$.

given the spectral resolution of the PCA and HEXTE, more sophisticated models like the above are poorly constrained and hence not warranted in this analysis. Nevertheless, as always, the spectral resolution of the detectors and the simplifying assumptions of the spectral models should be taken into account when one interprets the results of the analysis.

The top panel of Figure 2 shows the distribution of the observations as a function of the reduced $\chi^2_{\rm red} = \chi^2/{\rm d.o.f.}$ The peak of the distribution is at ~ 0.8 and for all observations $\chi^2_{\rm red} < 1.9$. The degrees of freedom (d.o.f. ~ 80) is large and this distribution should ideally be a narrow Gaussian centered at unity. However, the peak of the distribution is at ~ 0.8 instead of ~ 1. On the other hand, there are a few observations where $\chi^2_{\rm red}$ is too high. If we include more spectral components or parameters to the model, these high values of $\chi^2_{\rm red}$ may become acceptable, but the peak of the distribution will shift still lower than 0.8 and the analysis would severely suffer from over-modeling. Hence, the level of model sophistication used here may be close to optimal. To see if the observations with large values of $\chi^2_{\rm red}$ are biasing the analysis, in the bottom panel of Figure 2 we plot the best fit Γ values for the corresponding $\chi^2_{\rm red}$. While there is a tendency for spectra with higher Γ to have larger $\chi^2_{\rm red}$, the effect is not severe. We have checked that the observations with $\chi^2_{\rm red} > 1.5$ are removed from the sample; the results described in the next section are not affected.

4 RESULTS

The high energy photon index Γ of the thermal Comptonized component was the best constrained parameter and hence we study its correlation with other parameters. Moreover, Γ is a good indicator of the spectral state of the system and changes smoothly from the soft to hard states (Gierlinski et al. 2010). For the PCA data analyzed here, we plot Γ versus time in Figure 3. The data cover a wide time range and sample the various state transitions as well as the "failed" or partial transitions when $\Gamma < 2$.
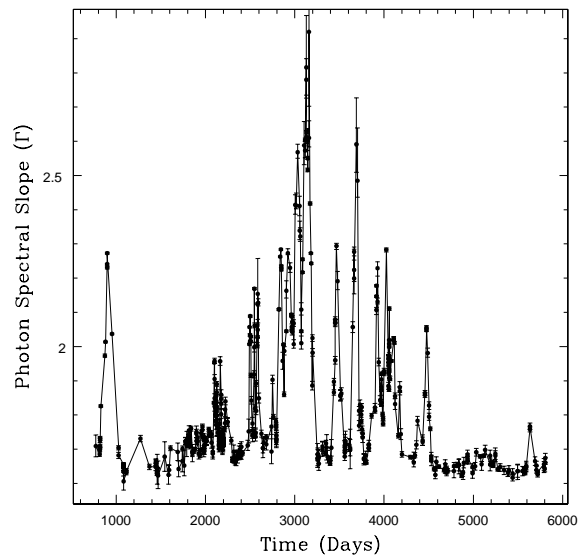
Fig. 3 The variation of photon spectral index with time for the pointed PCA observations analyzed in this work.
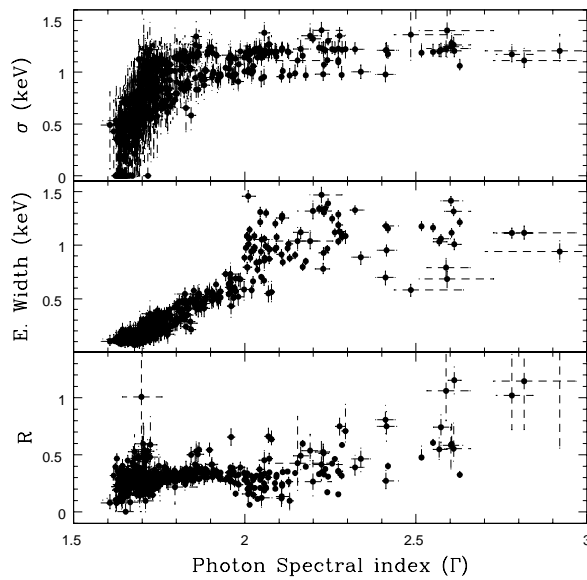

Fig. 4 The width σ (*Top Panel*), the Equivalent Width (*Middle Panel*) of the iron line and the reflection parameter R versus the photon spectral index Γ. For three observations, $R > 2$ and hence they are not plotted in the *Bottom Panel*.
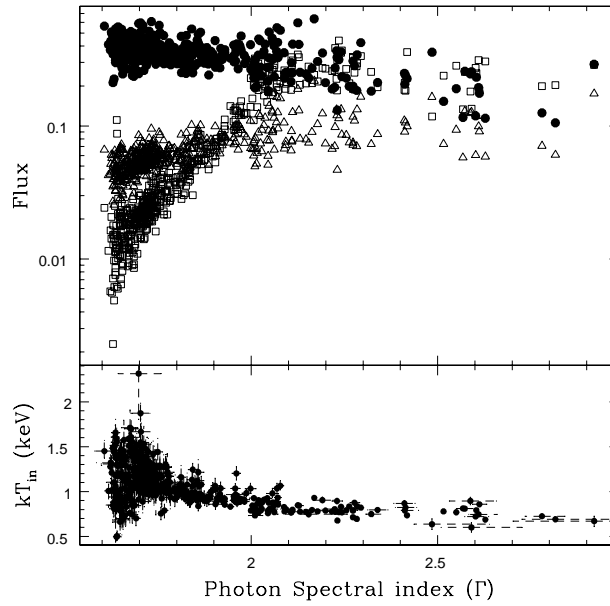
Fig. 5 *Top Panel*: The bolometric flux (10^{-7} erg cm^{-2} s^{-1}) versus the photon spectral index Γ. The circles represent the flux of the Comptonization component F_c, while the squares represent the flux of the disk's black body component, F_{DBB}. The triangles represent the flux of the input photons entering the Comptonizing region, F_{in}. *Bottom Panel*: The inner disk temperature kT_{in} versus Γ.

The width σ, the relative strength of the iron line and the reflection parameter R have been plotted versus Γ in Figure 4. The relative strength of the iron line (i.e. the Equivalent Width) correlates tightly with Γ for $\Gamma < 2.0$. There is a sharp change of behavior at $\Gamma \sim 2$ and for larger Γ values the Equivalent Width is uncorrelated and has a larger dispersion. The width of the line shows a similar behavior, being correlated at low $\Gamma < 1.8$ but uncorrelated for larger values. There is a hint of double valued solutions for the width versus Γ but given the errors it is difficult to make any concrete statements. If the iron line emission and the reflection component are from the same physical component, they should be correlated and indeed the reflection parameter R is also broadly correlated with Γ, as expected. However, the dependence is more complex with R having a non-monotonic behavior; there seems to be anti-correlation when $1.8 < \Gamma < 2.1$.

The top panel of Figure 5 shows the unabsorbed bolometric flux of the Comptonization component, F_c (filled circles), disk black body component, F_{DBB} (open squares) and that of the input photons entering the Comptonizing region, F_{in} (open triangles). As expected, the Comptonization component dominates during the hard state, while in the soft state, its flux is comparable with that of the disk's black body. It is interesting to note that the flux of the disk's black-body photons entering the Comptonization region is smaller than the observed disk black body flux in the soft state, but is larger in the hard state. This may indicate changes in the geometry of the system as discussed in the next section. The variation of the inner disk temperature kT_{in} is shown in the bottom panel of Figure 5. The temperature is nearly constant with a hint of an increase in the hard state.

The top panel of Figure 6 shows the Compton amplification factor $A = F_c/F_{in}$ which depends on Γ, kT_{in} and the hot electron temperature kT_e. In this modeling, $kT_e = 100$ keV is fixed. The solid lines depict the variation of A for a fixed value of $kT_{in} = 1.0$ keV (upper curve) and 0.5 keV
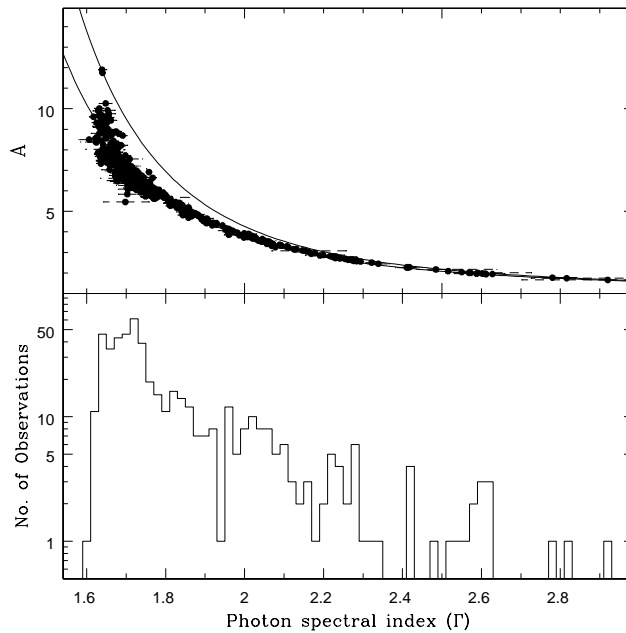
Fig. 6 *Top Panel*: The Compton amplification factor $A = F_{\rm c}/F_{\rm in}$ as a function of Γ. The lines represent the cases when $kT_{\rm in} = 1.0$ keV (*bottom line*) and $= 0.5$ keV (*upper line*). *Bottom Panel*: The distribution of observations as a function of Γ. Note that the sharp decline in number for $\Gamma < 1.65$ coincides with the steep increase in the amplification factor.

(lower curve). Variations in $kT_{\rm e}$ would shift these curves vertically. The estimated variation of A rises more steeply for smaller Γ than for the case when $kT_{\rm in}$ is a constant. This implies that in the hard state, as the required amplification increases, the system adjusts by decreasing Γ and $kT_{\rm in}$. The bottom panel of the figure shows the distribution of observations with Γ. Note that there is a sharp decline in the number of sources having $\Gamma < 1.65$ which is coincident with the steep increase in the amplification factor.

These results are broadly consistent with those of Wilms et al. (2006). In particular, for their thermal Comptonization model fitting, the width and strength of the iron line increases and saturates with decreasing Compton y-parameter, which is similar to the behavior described here as a function of the photon spectral index. They also found a similar trend for the reflection parameter R, however their results do not show any non-monotonic behavior as found in this work, which may be due to the larger number of observations analyzed in this work.

To re-emphasize that the results obtained here are subject to the validity of the Comptonization model used, we have analyzed 27 representative data sets with a broken power-law and a Gaussian model. The 23 observations represent the complete range of spectral index Γ obtained from the Comptonization model.

Figure 7 compares the reduced χ^2 for the broken power-law model and the Comptonization one used here. Clearly, the broken power-law model gives significantly larger reduced χ^2 than the Comptonization one. However as pointed out by Wilms et al. (2006), the systematic uncertainties of the PCA response does not allow for any concrete statements that the broken power-law model can be rejected. The top panel of Figure 8 shows the variation of the high energy photon index of the
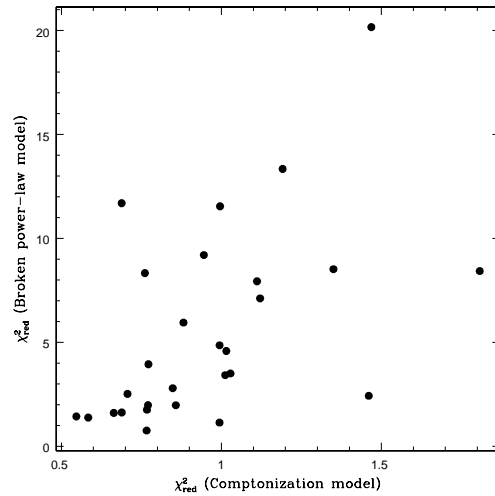
Fig. 7 Comparison of reduced χ^2 for the Comptonization model and the broken power-law one for 23 observations. The reduced χ^2 for the broken power-law is larger than that for the power-law, but the systematic uncertainty of the *RXTE* response does not allow for any concrete statements to be made.
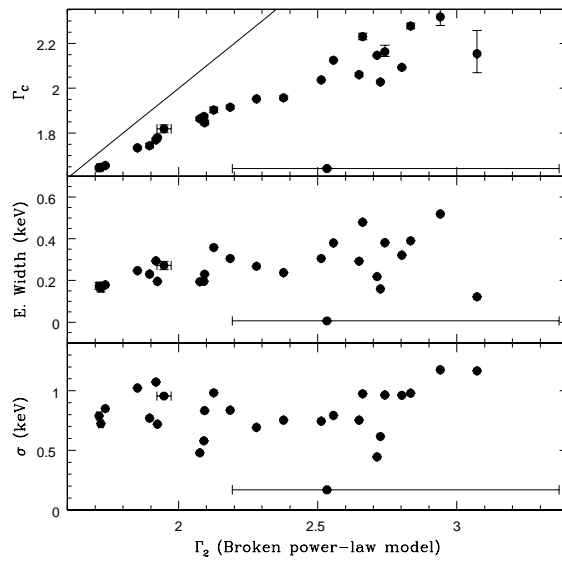

Fig. 8 *Top Panel*: The variation of the photon spectral index Γ_c from the Comptonization model used in this work with the high energy spectral index of the broken power-law model. While there is the expected correlation, the spectral index of the broken power-law model is systematically higher than the Comptonization one. *Middle and Bottom Panels*: The variation of the strength (Equivalent Width) and the width of the iron line versus the high energy power-law index for the broken power-law model. There is no clear correlation as was seen for the Comptonization model.

broken power-law model versus that of the Comptonization model. There is the expected correlation, but the broken power-law model indices are systematically higher. The middle and bottom panels of Figure 8 show the strength and width of the iron line versus the high energy photon index and no clear correlation can be seen. Thus, the correlations found in this work, for the Comptonization model, should be considered only within the framework of the model used. In other words, if the Comptonization model is assumed to be a good representative of the real physical radiative process, then the data suggest that there are correlations between the iron line parameters and the spectral index (Fig. 4).

5 DISCUSSION

An attractive and more or less standard model for Cyg X-1 is a geometrical one where for the hard state, there is a truncated disk surrounding a hot Comptonizing region in contrast to the soft state, where the disk extends to the inner regions and a hot corona on top Comptonizes its photons. During a state transition, the inner radius of the truncated disk moves inwards, while the inner Comptonizing region shrinks. As the cold disk fills the inner regions, a hot corona (or more specifically several active regions) arise on top of it and Comptonize its photons. The results presented here are broadly consistent with this general scenario, although there are some specific inconsistencies or complexities.

A natural consequence of this scenario is that as the inner radius of the disk moves inwards, the relative energy released between the inner hot region and the disk decreases. Hence, the required Compton amplification decreases which translates into an increase in the spectral index Γ. At the same time, the reflection parameter (and consequently the equivalent width of the iron line) should increase and so there should be a positive correlation between these quantities and Γ. Furthermore, as the disk moves inwards, the increased relativistic effects should broaden the iron line and hence the width of the line should also be correlated with Γ. As the disk fills the inner regions, the reflection and the line width should saturate to their maximum values, so in the soft state they should not be correlated with Γ.

These predictions are broadly consistent with the results shown in the top and middle panels of Figure 4. Both the relative strength (i.e. the Equivalent Width) and the width of the iron line increase with Γ and then saturate. However, the value of Γ for which this saturation occurs is different. Given the spectral resolution of the PCA and the approximate Gaussian model used for the skewed broad iron line, one may expect that the Equivalent Width is a better measured quantity than the width of the line. It is interesting to note that there is a rather sharp discontinuity in the Equivalent Width variation at $\Gamma = 2$. As the disk extends to the innermost region, the geometry of the Comptonization region changes from being a hot inner disk with $\Gamma < 2$ to a patchy corona on top of the disk with $\Gamma > 2$. This geometrical transformation at $\Gamma \sim 2$ could be the cause of the rather sharp discontinuity. The reflection parameter R has a complex non-monotonic behavior with Γ (Bottom Panel of Fig. 4). It is correlated for $\Gamma < 1.8$, inversely correlated for $1.8 < \Gamma < 2.1$ and correlated for larger values. This suggests that as the standard disk extends to the innermost radii, the geometry and nature of the active coronal regions become more complex and the disk may become ionized, an effect which is not taken into account here.

The top panel of Figure 5 shows the expected result that the flux of the Comptonizing components (filled circles) decreases with increasing Γ while the disk black-body flux increases (open squares). The flux of each of these components is single valued for a given Γ, which shows that the source *never* undergoes any hysteresis effect, confirming results obtained from a single transition (Zdziarski & Gierliński 2004). Such an effect has been observed in some black hole systems (e.g. GX 339–4) where the variation of Γ with flux depends on whether the source is transitioning from soft to hard or from hard to soft (Zdziarski & Gierliński 2004). It is interesting to note that for the entire soft state ($\Gamma > 2.0$) the disk emission is nearly equal to the Comptonizing one which implies

that the fraction of energy dissipated in the corona is ~ 0.5, independent of Γ. This is consistent with the results obtained from analysis of a single soft state data point in 1996 (Gierliński et al. 1999).

Here we demonstrate the universality of this result for different epochs of the soft state. It is also clear that Cyg X-1 never exhibits an ultra-soft state spectrum where the disk emission dominates the Comptonized one. The input flux of soft photons entering the Comptonized region are marked as open triangles in the top panel of Figure 5. For $\Gamma > 2.0$, this flux is less than the disk emission, which suggests that in the soft state the corona is a patchy one, covering a fraction of the surface area of the disk. These patchy active regions only Comptonize a fraction of the disk photons while the rest are directly observed. For the hard state ($\Gamma < 1.8$), it is surprising to note that the input photons have significantly more flux than the disk emission.

In the truncated disk geometry, one would expect a similar flux of disk photons entering into the inner Comptonizing region to what is directly observed. This may indicate that the truncated disk perhaps penetrates the inner hot region. The temperature of the inner disk kT_{in} (Bottom Panel of Fig. 5) also shows an unexpected behavior. In the soft state the temperature should be roughly constant, but as the disk recedes in the hard state, kT_{in} is expected to decrease. An opposite trend is observed with kT_{in} increasing with decreasing Γ, albeit with a large scatter. Although such high input disk temperatures for the hard state have been reported by Nowak et al. (2011), the presence of a soft excess, which may be due to an additional Comptonization component (Ibragimov et al. 2005), makes interpreting the results difficult. Another possibility is that the temperature of the inner disk and the seed photon temperature, which are assumed to be same in the model fitting, may not be equal. Moreover, it should be noted that these results are based on energies > 3 keV and on simple empirical spectral fitting models and hence need to be confirmed by a detailed broadband spectral fitting.

The amplification factor shows the expected trend of increasing sharply with decreasing Γ in the hard state (Top Panel of Fig. 6). It is interesting to note that this increase is slightly sharper than the expected curves when kT_{in} is held constant (solid lines). As the truncated disk recedes, the relative energy dissipation between the inner region and the disk increases, which requires a larger amplification factor A for energy balance. However, as can be inferred from the figure, the larger A requirement does not necessarily correspond to a significant change in Γ. For a range of $A > 7$, the spectral index $\Gamma \sim 1.65$. This naturally explains the absence of spectra with $\Gamma < 1.6$ seen in the distribution of Γ (Bottom Panel of Fig. 6).

In summary, the comprehensive spectral analysis of Cyg X-1 using 504 pointed observations is broadly consistent with the picture that in the hard state there is a truncated disk and a hot inner region. As the system moves to the soft state, the inner radius of the disk moves inwards. Finally in the soft state, the hot inner region disappears, with the appearance of active coronal regions on top of the cold disk. This scenario is supported by the increase of the relative strength and width of the iron line with spectral slope Γ for small values of $\Gamma < 2$ in the hard state and their saturation for large $\Gamma > 2$ values in the soft state. However, the reflection parameter R shows non-monotonic behavior with Γ, indicating complexities in the geometry or in the ionization state of the reflector. The analysis confirms that in the soft state the disk flux is similar to the Comptonized component for a large range of $2 < \Gamma < 2.9$ and the source never goes into an ultra-soft state. The input photon flux in the soft state is significantly smaller than the disk emission, indicating a patchy corona geometry. The inner disk temperature remains nearly constant at the soft state but unexpectedly shows an increase in the hard state, albeit with large scatter. The Compton amplification factor increases steeply with Γ, providing a natural explanation for the absence of any spectra with $\Gamma < 1.6$.

Finally, no hysteresis effect is detected, with the spectral index Γ being uniquely correlated with other parameters including the flux. The inconsistencies or complexities from the standard paradigm, indicated in this work, need to be confirmed by sensitive broad band instruments, especially those covering the spectrum at lower energies of $E < 3$ keV. Correlated temporal analysis with a theoretical understanding of the variability may also provide valuable insight into the nature of the system.

Overall, with its relative simplicity compared to other black hole systems, particularly transient ones, Cyg X-1 remains a promising source to understand the nature of accreting black hole systems.

References

Axelsson, M., Borgonovo, L., & Larsson, S. 2005, A&A, 438, 999

Belloni, T., Mendez, M., King, A. R., van der Klis, M., & van Paradijs, J. 1997, ApJ, 488, L109

Done, C., Gierliński, M., & Kubota, A. 2007, A&A Rev., 15, 1

Dunn, R. J. H., Fender, R. P., Körding, E. G., Belloni, T., & Cabanac, C. 2010, MNRAS, 403, 61

Esin, A. A., Narayan, R., Cui, W., Grove, J. E., & Zhang, S.-N. 1998, ApJ, 505, 854

Feng, Y. X., & Cui, W. 2002, ApJ, 564, 953

Gierlinski, M., Zdziarski, A. A., Done, C., et al. 1997, MNRAS, 288, 958

Gierliński, M., Zdziarski, A. A., Poutanen, J., et al. 1999, MNRAS, 309, 496

Gierlinski, M., Zdziarski, A. A., & Done, C. 2010, arXiv:1011.5840

Haardt, F., Maraschi, L., & Ghisellini, G. 1994, ApJ, 432, L95

Ibragimov, A., Poutanen, J., Gilfanov, M., Zdziarski, A. A., & Shrader, C. R. 2005, MNRAS, 362, 1435

Jahoda, K., Markwardt, C. B., Radeva, Y., et al. 2006, ApJS, 163, 401

Kotov, O., Churazov, E., & Gilfanov, M. 2001, MNRAS, 327, 799

Liang, E. P. T., & Price, R. H. 1977, ApJ, 218, 247

Lyubarskii, Y. E. 1997, MNRAS, 292, 679

Malzac, J., Petrucci, P. O., Jourdain, E., et al. 2006, A&A, 448, 1125

Misra, R. 2000, ApJ, 529, L95

Misra, R., Chitnis, V. R., Melia, F., & Rao, A. R. 1997, ApJ, 487, 388

Misra, R., & Zdziarski, A. A. 2008, MNRAS, 387, 915

Narayan, R., & Yi, I. 1994, ApJ, 428, L13

Nowak, M. A., Vaughan, B. A., Wilms, J., Dove, J. B., & Begelman, M. C. 1999, ApJ, 510, 874

Nowak, M. A., Hanke, M., Trowbridge, S. N., et al. 2011, ApJ, 728, 13

Pottschmidt, K., Wilms, J., Nowak, M. A., et al. 2003, A&A, 407, 1039

Remillard, R. A., & McClintock, J. E. 2006, ARA&A, 44, 49

Shapiro, S. L., Lightman, A. P., & Eardley, D. M. 1976, ApJ, 204, 187

Titarchuk, L., Shaposhnikov, N., & Arefiev, V. 2007, ApJ, 660, 556

Wilms, J., Nowak, M. A., Pottschmidt, K., Pooley, G. G., & Fritz, S. 2006, A&A, 447, 245

Zdziarski, A. A., & Gierliński, M. 2004, Progress of Theoretical Physics Supplement, 155, 99

Zdziarski, A. A., Johnson, W. N., & Magdziarz, P. 1996, MNRAS, 283, 193

Życki, P. T., Done, C., & Smith, D. A. 1999, MNRAS, 309, 561